Calculation of Liquid Loads Response to Forced Roll with Smoothed Particle Hydrodynamics

Louis Delorme, *Technical University of Madrid (UPM)*

Luis Casasús, *Technical University of Madrid (UPM)*

Luis Pérez-Rojas, *Technical University of Madrid (UPM)*

Antonio Souto-Iglesias, *Technical University of Madrid,*

ABSTRACT

In the last decade, Smoothed Particle Hydrodynamics (SPH) method has been paid an increasing attention, especially when simulating liquid motions. In this article, the method is applied to passive stabilizer tanks for vessels. Highly non linear motion of the free surface can happen in these tanks, including breaking waves and wave impacts on the walls. The advantage of SPH is that it can deal more efficiently with such phenomena than the methods using a grid. In Souto et al. (2004), both numerical and experimental investigation on passive stabilizer tanks were presented. Results were promising, resonance phenomena were reproduced, but further investigations were needed, especially on the pressure field near the walls that is a critical point when designing those tanks, or containers.

In this article, a new experimental setup for roll motion for a fishing vessel tank geometry is described in detail. A torsiometer measures the moment with respect to the rolling axis and the phase lag is calculated with respect to the angle signal. Amplitude and phase lag of the moment are presented for a wide range of oscillation frequencies, including the first sloshing frequency of the tank and the resonance roll frequency of the ship.

Experimental and numerical results are compared. Numerically, the SPH method is presented with an emphasis on the solid boundary treatment. Efficiency of the boundary simulation is discussed.

Keywords: *SPH, Sloshing, LNG, passive anti-roll tanks*

1. INTRODUCTION

The presence of free surface tanks in a marine structures generates wave loads that affect its behaviour and becomes an important issue when designing those structures. The goal can be to reduce the loads caused by the water in the tank, as it is the case for LNG vessels (Tveitnes et al., 2004), or to get an appropriate counter balance moment in the case of the design of passive anti-roll tanks (Bass, 1998). Highly non linear phenomena in the tanks, known as sloshing phenomena, play a dominant role and need a specific study.

The sloshing problem has been studied over the last fifty years following different approaches. Linear potential flow (Graham & Rodriguez, 1952) and non linear one based on a modal decomposition of the free surface

(Faltinsen et al., 2005) have been used. These techniques provide fast results but do not allow the modelling of phenomena as overturning waves or shallow water tanks. In the last 20 years, numerical methods have been applied to sloshing, solving the Navier-Stokes equations by means of finite difference scheme (Frandsen, 2004), VOF method (Sames, 2002), or Smoothed Particle Hydrodynamics (Landrini et al., 2003). SPH is an interesting alternative method to traditional grid-based methods since its Lagrangian character allows the simulation of high deformations of the free surface including overturning waves.

This article presents experimental results for the case of a passive stabilizer tank. The new experimental device is first described. The moment created by the water over the rolling axis is measured and the analysis is done on its first harmonic (corresponding to the tank motion).

Those results are compared with SPH simulations. SPH formulation is presented with an emphasis on the boundary treatment. Both moment and free surface shapes are compared for a wide range of excitation frequencies of the tank.

2. EXPERIMENTAL SETUP

The experimental device consists of a high precision torsiometer with a 200 Nm range, a structure that holds the tank, and an electrical engine that produces a harmonic rolling motion on the tank.

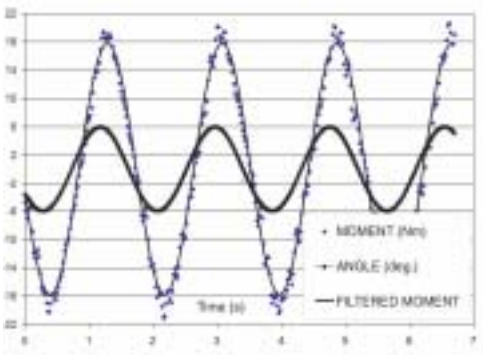

Figure 1 Experimental data obtained for each excitation frequency. Units of the vertical axis are degrees for the angle curve and N.m for the moment curves

The moment and angle signal are registered, filtered and processed (figure 1) and the amplitude and phase lag of the filtered moment represents the data that is to be compared with the numerical simulation. Filtering the moment data by extracting its most important harmonic is the standard procedure employed when using experimental data for projecting and tuning the anti-roll systems. We will proceed in the same way when performing the analysis of the numerical results.

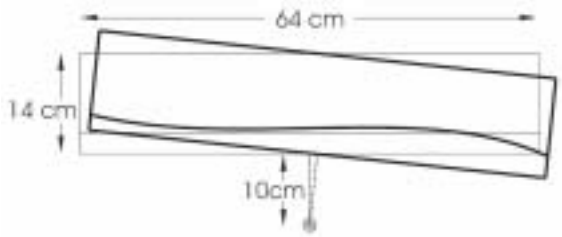

Figure 2 Geometry of the tank

The geometry of the tank is shown in figure 2. It is a rectangular tank with a breadth B = 64cm and a height of 14cm. All the results are given for a width of 25.2cm. The rotation axis is 10cm below its baseline. The maximum rotation angle is 6 degrees.

The water depth h used in this study is 3cm, which means that h/B = 0.047, and hence the case is a shallow water one. The corresponding first resonance frequency can be obtained from the linear wave theory. In this case, its value is $\omega_0 = 2.65 rad/s$. The frequency range used goes from 0.24 to 8.21 rad/s, with a step of 0.26 rad/s. The graph of the amplitude of the filtered experimental moment for this range of frequencies is shown in figure 3. The first resonance frequency almost corresponds to the maximum value of the amplitude, as it should be in these circumstances.

In figure 3, we can notice dramatic variations in the curve shape depending on the frequency, mainly between points A and B,

corresponding to $\omega_A = 4.34 rad/s$ and $\omega_B = 4.87 rad/s$. When the frequency of the movement is so high that the wave can not follow the movement, the moment amplitude falls dramatically. This transition happens between points A and B. We can observe this effect by the shape of the free surface for both cases in figure 4. In picture A the wave develops completely and clashes with the tank top. In picture B, the wave travelling to the right clashes with another one going to the left and thus breaks before reaching the end of the tank.

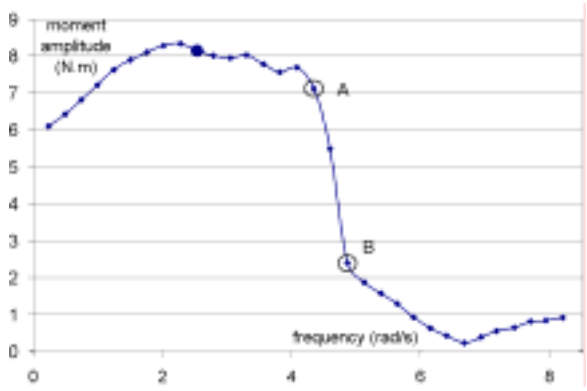

Figure 3 Experimental values of the moment amplitude (N.m) for the test case, as a function of the excitation frequency (rad/s). The solid round marker corresponds to the closest point to the first resonance frequency. Points A and B refer to figure 4

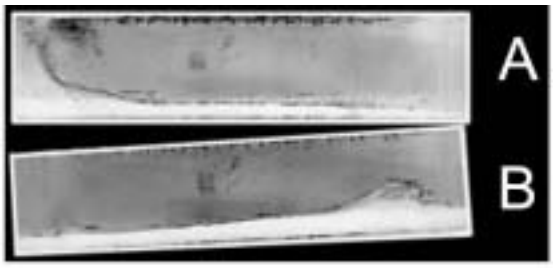

Figure 4 Pictures A and B correspond to points A and B in figure 3

3. SPH FORMULATION OF THE PROBLEM

3.1 SPH Formalism

Smoothed particle hydrodynamics (SPH) is a method for obtaining approximate numerical solutions of the equations of fluid dynamics by replacing the fluid by a set of particles. In SPH, the formulation is Lagrangian, allowing to deal with the equations of the problem without the convective terms. No free-surface condition is needed in SPH because the particles implicitly define the free-surface position. On the other hand, an additional term is needed in the momentum equation to guarantee solid boundary conditions. This is one of the critical point of SPH. A very good review paper has been recently published by Monaghan, (Monaghan, 2005), complementing a previous one by the same author (Monaghan, 1992).

$$\langle \mathbf{f}(\mathbf{r}) \rangle = \int_{\Omega} \mathbf{f}(\mathbf{r}') \, W(|\mathbf{r} - \mathbf{r}'|, h) \cdot d\Omega \qquad (1)$$

in which $\boldsymbol{\Omega}$ is the fluid domain. In the integral (1) the function *W* is called the kernel. The kernel depends on the distance between particles and on a distance *h* called the smoothing length, indicating the range of influence of a particle. A cubic spline kernel (Monaghan, 2005) has been used in the 2D simulations presented in this article.

Assuming the function **f(r)** to be known at a discrete set of *N* spatial points, indexed by *i* and *j*, the equation (1) can be approximated by:

$$\langle \mathbf{f}(\mathbf{r}_i) \rangle \approx \sum_{j=1}^{N} \mathbf{f}(\mathbf{r}_j) W(\mathbf{r}_{ij}, h) \cdot V_j \qquad (2)$$

where V_j represents the volume (or surface in two dimensions) associated to the point r_j and $r_{ij} = | r_i - r_j |$. If the point r_i represents a particle of mass m_j and density ρ_j, its volume is $V_j = m_j / \rho_j$.

The gradient of any vector function **f(r)** is obtained by integrating by parts equation (1) neglecting the surface integral and discretizing on the set of particles, giving:

$$\langle \nabla \mathbf{f}(\mathbf{r}_i) \rangle \approx \sum_{j=1}^{N} \mathbf{f}(\mathbf{r}_j) \nabla W(\mathbf{r}_{ij}, h) \frac{m_j}{\rho_j} \qquad (3)$$

3.2 Application to Incompressible Fluids

The SPH formalism is applied to the Navier Stokes equations in order to simulate fluid motions. The continuity equation becomes (Monaghan, 2005):

$$\frac{d\rho_i}{dt} = \sum_j m_j \left(\mathbf{v}_i - \mathbf{v}_j\right)\nabla_i W\left(\mathbf{r}_{ij}, h\right) \qquad (4)$$

One should note that the density of a particle could be obtained by directly applying equation (2) to the density. Nevertheless, this expression gives a vanishing density field near the free-surface.

There are different ways to apply the SPH formalism to the momentum equation of an inviscid fluid. The simplest way to guarantee momentum conservation is making the interaction between two particles symmetric. Following Monaghan, 1994, an additional symmetric term π_{ij} is introduced in the momentum equation to model the dissipation due to viscous forces and to stabilize the numerical method, equivalent to the artificial viscosity term that dampens spurious oscillations in finite difference schemes. The momentum equation written for a generic particle *i* is:

$$\frac{d\mathbf{v}_i}{dt} = -\sum_j m_j \left(\frac{P_i}{\rho_i^2} + \frac{P_j}{\rho_j^2} + \Pi_{ij}\right)\nabla_i W\left(\mathbf{r}_{ij}, h\right) + \mathrm{g} \qquad (5)$$

Different forms of the viscous term π_{ij} have been proposed. We will use the one of Monaghan (Gray, 2001).

$$\Pi_{ij} = -\alpha \frac{c_s \mu_{ij}}{\bar{\rho}_{ij}} \qquad (6)$$

$$\mu_{ij} = \frac{h \cdot \mathbf{v}_{ij}\mathbf{r}_{ij}}{(r_{ij} + \eta)^2} \qquad (7)$$

where $\bar{\rho}_{ij}$ is the average density of particles *i* and *j*. $\mathbf{v_{ij}}$ represents the velocity difference between particles *i* and *j* and c_s is the numerical sound speed. α is a viscosity parameter. η is a parameter included to avoid singularity when the particles get very close. Results presented here were obtained with $\eta = 0.01h^2$ and α =0.02.

Impose incompressibility directly can be done by solving a Poisson equation for the pressure. Nevertheless, its high cost and the necessity to define explicitly the free surface in order to apply boundary condition on it make that a common practise in SPH is to consider the fluid as compressible and assume a stiff equation of State. For a particle i :

$$P_i = \frac{c_s \rho_0}{\gamma}\left(\left(\frac{\rho_i}{\rho_0}\right)^{\gamma} - 1\right) \qquad (8)$$

where ρ_0 is the reference density and γ is taken as 7 (Batchelor, 1967).

The relative density variation in the fluid is proportional to the square of the Mach number (Monaghan, 1994). Nevertheless, the sound speed influences the time steps used in the time integration through the Courant condition. Hence, a common practise is to choose the sound speed such that the density variation is not bigger than 1%, because smaller density variations would induce much shorter time steps.

3.3 Solid Boundary Treatment

In SPH the free surface is defined implicitly by the position of the particles. Hence no free surface boundary condition is required. Nevertheless, this becomes problematic when dealing with solid boundaries. Since no fluid particle is located on the boundary, it is difficult to impose free-slip/no slip condition on them.

A first possibility to treat the solid boundary is to consider that a particle getting closer to a wall suffers an inelastic bounce loosing a part of its kinetic energy. This techniques lacks precision and introduce distortion in the flow.

In the last 5 years, some authors have used ghost particles (Colagrossi et al., 2003), formed by reflecting the fluid particles on the other side of the boundaries. These ghost particles are defined with the same density, same pressure and opposite velocity of the reflected particles. These ghost particles are then taken into account in the equations (4) and (5) and act as a repulsive boundary force. This way of proceeding is more intuitive and works quite well. Nevertheless, it becomes very difficult to implement when the geometry is complex.

Alternatively, boundary particles can be placed on the walls, exerting a repulsive force on the fluid particles (Monaghan & Kos, 1999). This repulsive force enters in the momentum equation (5) and had initially the form of a Lennard-Jones force, due to the analogy between SPH with molecular dynamics.

SPH results presented in this article are obtained with boundary particles placed on the wall exerting on the fluid a force derived from the gradient of the kernel (Gray, 2001), but instead of the gradient of the kernel we used :

$$F_b(u) = f\begin{cases} \dfrac{2}{3} & if \quad 0 < u < 2/3 \\ 2u - \dfrac{3}{2}u^2 & if \quad 2/3 \le u \le 1 \\ \dfrac{(2-u)^2}{2} & if \quad 2 \le u \le 1 \\ 0 & if \quad u \ge 2 \end{cases} \qquad (9)$$

Where $u = r_\perp / h$, h is the smoothing length, $r_\perp$ is the perpendicular distance between the particle and the solid boundary, and f is proportional to the square of the sound speed. Our proportionality constant is 0.01, i.e., $f = 0.01 c_s^{\,2}$.

Figure 5 shows the function $F_b(r)$ and the gradient of the kernel used in the simulations. The value of $F_b(r)$ between $r=0$ and where the gradient reaches its maximum value has been changed to a constant. This makes that the final boundary force does not tend to 0 when $r_\perp$ tends to 0, avoiding penetration of the boundary.

To ensure that a particle moving parallel to a boundary suffers a constant force from the set of boundary particles, the boundary force magnitude F_b is multiplied by **an** interpolation function P, depending on the tangential distance $r_{//}$ between the fluid particle and the boundary particle. The final boundary force we use has the following form (Gray, 2001).

$$\boldsymbol{F} = F_b(r_\perp) P(r_{//}) \boldsymbol{n} \qquad (10)$$

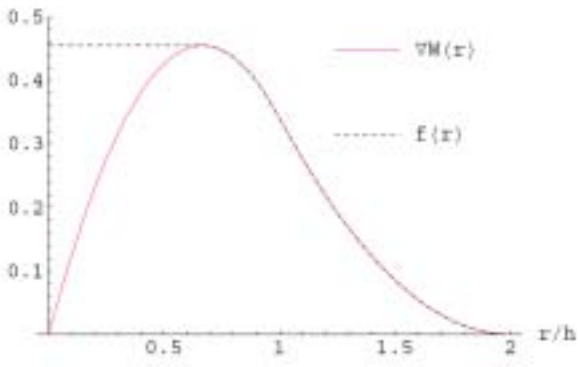

Figure 5 Gradient of the kernel and function $F_b(r)$ in the boundary force. Units of the vertical axis are m^{-3} for the gradient of the kernel and N for the function f(r).

where $\boldsymbol{n}$ is the normal vector of the boundary oriented towards the fluid domain. The interpolation function takes the following form:

$$P(r_{//}) = \frac{1}{2}\left(1 + \cos\left(\frac{\pi r_{//}}{\Delta p}\right)\right) \qquad (11)$$

with Δp the separation between two consecutive boundary particles.

3.4 Moment over the rolling axis

In order to calculate the global moment exerted by the fluid over the rolling axis, the value of the pressure can be interpolated and integrated over the tank walls. Nevertheless, the interpolated values lack of precision and we used the boundary particles to calculate the global moment. If $\boldsymbol{f}_a$ is the forced exerted by a boundary particle $\boldsymbol{a}$, the sum of $\boldsymbol{f}_a$ over all the boundary particle is the force of the tank on the fluid to maintain it, i.e. the opposite of the force exerted by the fluid on the tank. As a consequence, the moment M_1 created by the fluid over the rolling axis is :

$$M_1 = -\sum_{a \in BP} \boldsymbol{f}_a \wedge \boldsymbol{r}_a \qquad (12)$$

As experimentally done, once a temporal evolution of M_1 is obtained, a Fourier analysis is done for each excitation frequency in order to obtain the component of the moment of the same frequency as the excitation one. Amplitude and phase lag of this moment with respect to the motion of the tank will be compared.

3.5 Time Integration Scheme

A leap frog predictor-corrector scheme is used in the simulations. The positions of the particles are calculated with an explicit second order scheme and both velocity and density are predicted and afterwards corrected (Gray, 2001).

The time step is defined by the minimum result obtained from three different criteria related with a Courant stability condition:

Gravity time step: $\Delta t_1 = 0.5\sqrt{h/g}$

Viscous time step: $\Delta t_2 = 2h/c_s(2+\alpha)$

Boundary particle forces time step:

$$\Delta t_3 = 0.5 \min\{r_\perp / \sqrt{0.01 c_s^2}\}$$

The last time step condition is usually the most restrictive one. With 2500 fluid particles and 500 boundary particles, the average time step is 1 e-4 with a sound speed of 25 m/s. CPU time (Pentium 3GHz) is about half an hour for 1 second of simulation time.

4. VALIDATION OF SPH RESULTS

4.1 Phase Lags

In the case of a stabilizer tank, the most important data relative to the water motion in the tank is the phase lag between the moment created by the water over the rolling axis and the motion of the tank. A 90 degrees phase lag means that the moment created by the liquid acts in opposition to the motion and that the tank gets a maximum stabilizing effect. The goal of the design of stabilizer tanks is that this 90 degrees phase lag is reached at the roll natural resonance frequency of the ship.

Figure 6 presents the phase lag curve for the test case presented in section 2 in which a wide range of frequencies, including the roll natural frequency of the ship, is studied.

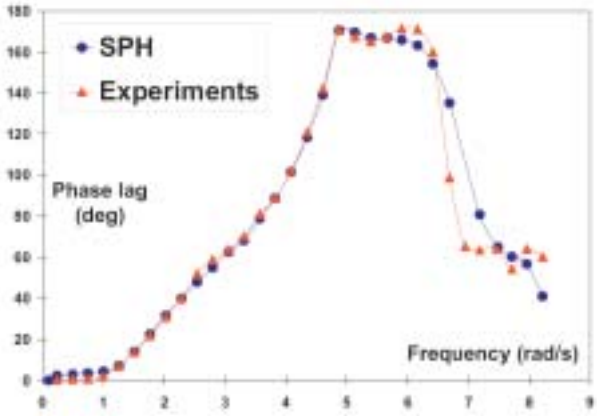

Figure 6 Experimental vs SPH simulation phase lag curves

The similarity between the numerical and experimental values is very good for the frequencies close to the first natural frequency of the flow motion $\omega_0 = 2.65 rad/s$. There is a lack of accuracy for the highest frequencies where the motion starts to become chaotic and

the amplitude of the experimental data is smaller, a fact that always affects accuracy.

4.2 Moment Amplitudes

The magnitude of the moment exerted by the water on the tank is necessary to quantify the effects of the stabilizer tank on the ship.

The comparison of experimental and simulation values of the moment amplitude for the test case is shown in figure 7. The agreement is good for most of the points, except for frequencies just below 4 rad/s. These points need further research. We present a comparison with the results of Verhagen 1963, that are meant to be accurate for the region close to the first resonance frequency.

It is very interesting to notice that the simulation reproduces all the changes in the tendencies of the experimental data, including the dramatic fall of moment amplitude for $\omega \approx 4.5$ described earlier. It is also interesting to notice that for the highest frequencies, the method keeps the error within a narrow gap, although the phase lags are not so accurate in this part of the curve, as we have already commented above.

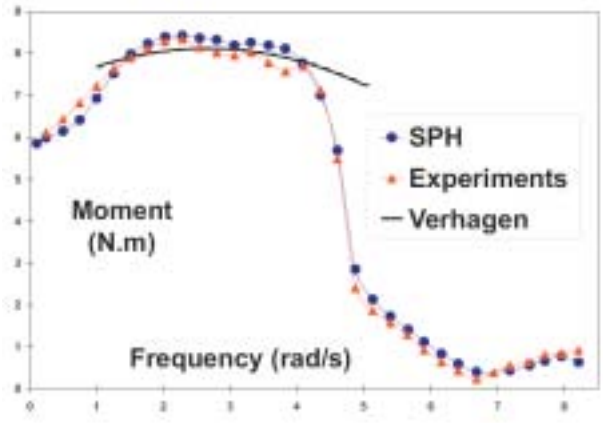

Figure 7 Experimental vs SPH simulation moment amplitude curves

4.3 Phase Diagrams

Figure 8 shows the phase diagram which is aimed at simultaneously comparing moment amplitude and moment phase lag. The horizontal component of every point is obtained by projecting the moment amplitude with the cosine of the phase lag. Hence, the horizontal component is the part of the response that follows the motion. The vertical component is obtained by projecting the moment amplitude with the sine of the phase lag. Hence, it is the part of the response that counteracts the motion. Both have to be analyzed when designing a passive stabilizer tank. The agreement is very good for most of the points but errors cannot be neglected when the phase lag is around 90º. This phase lag corresponds to frequencies just below 4 rad/s, where the errors in the momentum amplitude are bigger.

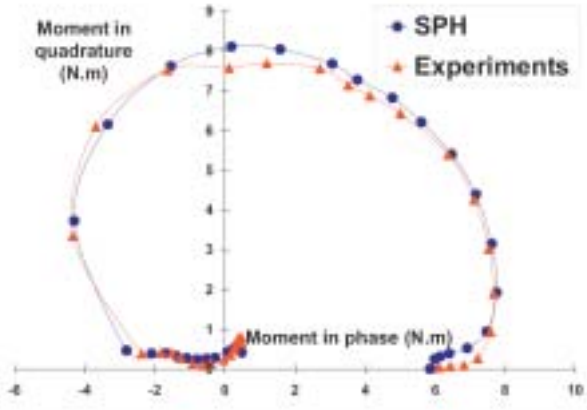

Figure 8 Experimental vs SPH simulation moment phase diagrams

4.4 Free Surface Shape

Although it has no quantitative character, it is very interesting to compare experimental and numerical free surface shapes in order to check whether the general dynamics of the flow correspond to the experimental ones. The images from the numerical calculation are obtained by placing scaled velocity vectors at the position of the particles.

Figures 9 and 10 show free surface at rolling angle $\alpha = 0^{o}$ for excitation frequencies $\omega = 4.34 rad/s$ and $\omega = 4.87 rad/s$ (points A and B on figure 3). There is a clear lack of resolution regarding the splash and breaking but the general dynamic is very well

reproduced, thus justifying the accuracy of the global result regarding phase lag and moment.

At frequency $\omega = 4.34 rad/s$, the lag is around 90 degrees (figure 6) and the main wave in the tank is in opposition of phase with respect to the tank motion (see figures 9 & 11). As a result the wave impacts periodically on the tank walls.

On the other hand, when the excitation frequency is much higher (point B for instance) than the resonance one, the main wave in the tank does not travel fast enough to impact on the walls and a smoother behaviour is observed. It confirms the reduction of the moment amplitude after resonance (figure 7).

Figure 9 $\omega = 4.34 rad/s$, $\alpha = 0^o$

Figure 10 $\omega = 4.87 rad/s$, $\alpha = 0^o$

Figures 11 and 12 present the same excitation frequency for the maximum roll angle $\alpha = 6^o$. Splash-up phenomenon is not well reproduced because of the lack of resolution. To have a better idea of the phenomenon, experimental videos, numerical ones, and superposition of both are available at http://canal.etsin.upm.es/papers/stab06.

Figure 11 $\omega = 4.34 rad/s$ $\alpha = 6^o$

Figure 12 $\omega = 4.87 rad/s$ $\alpha = 6^o$

5. CONCLUSIONS AND FUTURE WORKS

Sloshing in shallow water tank has been tested experimentally and reproduced numerically with SPH. The comparison of phase lags and moment amplitudes shows that the simulations reproduce very well this highly non linear phenomenon. Nevertheless, further work has to be done to improve the capacities of the simulation.

From an engineering point of view, local loads on the walls are of great interest. Thus, experimental and numerical values of pressure must thus be obtained and compared. Pressure is obtained in SPH from density with a very stiff equation of state and consequently small errors in density become very amplified and tend to occur when particles are close to the boundaries. Although some results for local pressure values in sloshing type problems with SPH have already been published (Landrini et al., 2003), they are far from being satisfactory. Research is needed in this field, focused on the solid boundary treatment with SPH.

Dissipation is a also a critical point of the method. A viscous term was included in the discretized momentum equation with the purpose of increasing the stability properties of the numerical algorithm. For long term simulations it is not clear how the value of this term affects the evolution. In addition, although it can be very important for medium-high frequencies, we do not consider the physical dissipation due to turbulence when the overturning waves splash and break. Therefore,

a better dissipation model is required that incorporates a turbulence model.

Finally, an uncertainty analysis of the experiments for the anti-roll tanks is needed. The sources of errors are diverse and a deep analysis is required to individualize and assess the extent of the errors produced by each source. The outcome of this analysis would be the establishment of an error uncertainty value for every experimental point.

6. ACKNOWLEDGMENT

This work has been partially funded by the program PROFIT 2005 of the Spanish Ministerio de Educación y Ciencia through the project STRUCT-LNG (file number CIT-370300-2005-16) leaded by the Technical University of Madrid(UPM).

7. REFERENCES

Bass, D.W., 1998, "Roll Stabilization for Small Fishing Vessels using Paravanes and Anti-Roll Tanks", Mar. Technol. SNAME N. 35(2), 74-84.

Batchelor, G.K., 1967, "An introduction to fluid dynamics", Cambridge University Press.

Colagrossi, A., Landrini, M., 2003 "Numerical simulation of interfacial flows by smoothed particle hydrodynamics", J.Comput. Phys. 191(1), 448-475

Faltinsen, O.M., Rognebakke, O.F., Timokha, A.N., 2005, "Resonant three-dimensional nonlinear sloshing in a square-base basin. Part 2. Effect of higher modes", J. Fluid Mech. 523, 199-218.

Frandsen, J.B., 2004, "Sloshing motions in excited tanks", J. Comput. Phys. 196(1), 53-87.

Gray, J., 2001, "Caldera Collapse and the generation of waves", Phd Thesis, Department of Mathematics and Statistics, Monash University. Australia.

Graham, E.W., Rodriguez, A.M. 1952, "The characteristics of fuel motion which affects airplane dynamics", J. Appl. Mech. 19, 381-388.

Landrini, M., Colagrossi, A., Faltinsen, O.M., 2003, "Sloshing in 2-D flows by the SPH method", Proc. 8th Int. Conf. on Numerical Ship Hydr., Busan, Korea.

Lucy, L.B., 1977, "A numerical approach to the testing of the fission hypothesis", Astron. J. 82(12), 1013-1024.

Monaghan, J.J., 1992, "Smoothed Particle Hydrodynamics", Annu. Rev. Astron. Astr. 30, 543-574.

Monaghan, J.J., 1994, "Simulating Free Surface Flows with SPH", J. Comput. Phys. 110(2), 399-406.

Monaghan, J.J., Gingold, R.A., 1983, "Shock Simulation by the Particle Method SPH", J. Comput. Phys. 52, 374-389.

Monaghan, J.J., Kos, A., 1999, "Solitary Waves on a cretan beach" J. Waterw. Port C. ASCE 125, 145–154.

Monaghan, J. J., 2005. "Smoothed Particle Hydrodynamics", Rep. Prog. Phys. ,68, 1703- 1759.

Sames, P.C., Marcouly, D., Schellin, T.E., 2002, "Sloshing in Rectangular and Cylindrical Tanks", J. Ship Res. 46(3), 186-200.

Souto Iglesias, A., Pérez Rojas, L., Zamora, R., 2004, "Simulation of anti-roll tanks and sloshing type problems with Smoothed Particle Hydrodynamics", Ocean Eng. 31(8-9), 1169-1192

Tveitnes, T., Ostvold, T.K., Pastoor, L.W., Sele, H.O., 2004, “A Sloshing Design Load Procedure for Membrane LNG Tankers”, Proc. 9th Symp. on Practical Design of Ships and Other Floating Structures. Luebeck-Travemuende, Germany.

Verhagen, J.H.G., Van Wijngaarden, L., 1965, “Non-linear oscillations of fluid in a container”, J. Fluid Mech. 22(4), 737-751.